Crisis-induced intermittency in two coupled chaotic maps: Towards understanding chaotic itinerancy

G. Tanaka,[1] M. A. F. Sanjuán,[2] and K. Aihara[1,3]
[1]*Department of Complexity Science and Engineering, Graduate School of Frontier Science, The University of Tokyo, Tokyo, 113-8656, Japan*
[2]*Nonlinear Dynamics and Chaos Group, Departamento de Matemáticas y Física Aplicadas y Ciencias de la Naturaleza, Universidad Rey Juan Carlos, Tulipán s/n, Móstoles, Madrid, 28933, Spain*
[3]*ERATO Aihara Complexity Modelling Project, JST, 45-18 Oyama, Shibuya-ku, Tokyo, 151-0065, Japan*
(Received 28 June 2003; revised manuscript received 23 July 2004; published 25 January 2005)

The present paper considers crisis-induced intermittency in a system composed of two coupled logistic maps. Its purpose is to clarify a bifurcation scenario generating such intermittent behaviors that can be regarded as a simple example of chaotic itinerancy. The intermittent dynamics appears immediately after an attractor-merging crisis of two off-diagonal chaotic attractors in a symmetrically coupled system. The scenario for the crisis is investigated through analyses of sequential bifurcations leading to the two chaotic attractors and successive changes in basin structures with variation of a system parameter. The successive changes of the basins are also characterized by variation of a dimension of a fractal basin boundary. A numerical analysis shows that simultaneous contacts between the attractors and the fractal basin boundary bring about the crisis and a snap-back repeller generated at the crisis produces the intermittent transitions. Furthermore, a modified scenario for intermittent behaviors in an asymmetrically coupled system is also discussed.

DOI: 10.1103/PhysRevE.71.016219 PACS number(s): 05.45.Ac, 05.45.Df

I. INTRODUCTION

Coupled chaotic systems show a rich variety of collective phenomena such as chaotic synchronization [1–4] and chaotic itinerancy [5–7]. The importance and interest in understanding collective dynamics of coupled chaotic systems lie in the fact that they are often used to model a group of interacting units such as biological networks and electronic circuits. The present paper considers a scenario leading to intermittent behaviors in a system composed of two coupled chaotic maps, aiming at better understanding chaotic itinerancy.

Chaotic itinerancy has been proposed as a concept to describe a dynamical state consisting of chaotic transitions among nearly ordered behaviors [6]. The mathematical foundation of this concept has been intensively studied [7]. Itinerant memory dynamics [8,9], or nonperiodic associative dynamics [10], found in chaotic neural networks [11] can be also considered as an example of chaotic itinerancy. The mechanism of the onset of itinerant memory dynamics in a system of four coupled chaotic neurons has been recently clarified in terms of global bifurcations [8,9]. Before a global bifurcation, four distant chaotic attractors symbolizing different memories are coexisting. A trajectory asymptotes to one of the attractors depending on the initial condition, i.e., the network recalls one of the memories. At the bifurcation point, the unstable manifolds of the unstable periodic points embedded in the attractors intersect and then a trajectory starts irregular itinerant transitions among the four originally attracting regions.

Similar transient dynamics is also found in a system of two coupled logistic maps. It corresponds to a dynamical phenomenon called *crisis-induced intermittency* [12,13]. The intermittent behavior appears immediately after simultaneous interior crises of two mutually symmetric off-diagonal attractors. This is called an attractor-merging crisis [12]. An advantage of using a two-dimensional map as a case study is that observations of basin structures can be easier and helpful for a better understanding of dynamical phenomena in higher-dimensional systems. With this in mind, the present paper studies the emergence of crisis-induced intermittency in a simple two-dimensional model. We analyze bifurcations of the two off-diagonal attractors and modifications of basins of attraction, i.e., basin bifurcations [14] or basin metamorphoses [15]. The noninvertible property of the model brings about a complicated basin structure. We use some techniques for analyses of chaotic dynamics and global bifurcations in two-dimensional noninvertible maps [14,16].

A process leading to merging of two mutually symmetric chaotic attractors has been studied in terms of basin bifurcations in Ref. [14]. The attractors simultaneously contact a *fractal basin boundary* [17] of their basins of attraction. We carry out a similar analysis of basins as well as quantitative characterization of the changes of basins with the dimension of the basin boundary in the two-dimensional model. Moreover, we discuss a modified scenario of basin bifurcations leading to intermittent behaviors in an asymmetrically coupled system to consider the robustness of the phenomena.

From another viewpoint, the attractor-merging crisis in the symmetrically coupled maps can be considered as a reunion of chaotic attractors [18]. This occurs because the crisis restores the symmetry that has been broken by a pitchfork bifurcation of a fixed point on the diagonal. Maistrenko *et al.* [18] have investigated two mechanisms of reunion of several pieces of a chaotic attractor into a one-piece chaotic attractor in a system of two-dimensional piecewise linear maps. A mechanism called a *contact bifurcation of the first kind* [19] gives rise to a sudden change of two or more pieces of some

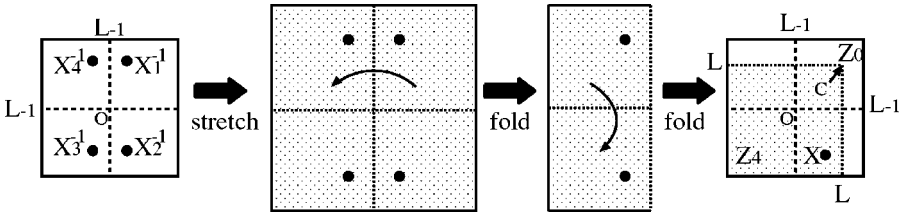

FIG. 1. Schematic illustration of the transformation T with $\epsilon=0$ for the phase plane. The phase plane is two-dimensionally stretched, and then folded with respect to the two axes. The critical curve L separates the two open regions, Z_0 where any point has no preimages and Z_4 where a point X has four rank-1 preimages X_i^{-1} $(i=1,2,3,4)$.

cyclic chaotic attractor into a larger chaotic attractor with the appearance of bursts. This type of reunion is brought about by a contact of chaotic pieces with a basin boundary. In piecewise linear maps [18], the contact occurs with a fractal basin boundary generated through a homoclinic bifurcation of a saddle cycle. In this case, the boundary embeds a *chaotic saddle*, i.e., a geometrically strange, invariant, nonattracting set, which is made up of an infinite number of unstable periodic orbits. In our case, the contact occurs with a fractal basin boundary that arises after a boundary crisis [20] of an attractor. A chaotic repeller, or a strange repulsor [14], is embedded in the fractal basin boundary.

The organization of the paper is as follows. In Sec. II, some properties of the system of two symmetrically coupled logistic maps are described with the critical curve, which is a useful tool for understanding a basin bifurcation [14]. In Sec. III, bifurcations of two mutually symmetric off-diagonal attractors are investigated and the parameter region where they coexist is specified. In Sec. IV, basin structures are examined with invariant manifolds of saddle cycles. In Sec. V, basin bifurcations are qualitatively investigated with the genesis, changes, and destruction of a fractal basin boundary. These changes in basin structures are also quantitatively characterized using variation of a dimension of the fractal basin boundary. In the last section, we discuss a modified scenario leading to intermittent behaviors in a system of two asymmetrically coupled logistic maps with a slight mismatch of the nonlinearity parameters.

II. THE MODEL AND ITS PROPERTIES

We consider a family of transformations T with two coupled logistic maps in the following form:

$$\begin{aligned} x_{n+1} &= (1-\epsilon)f_\lambda(x_n) + \frac{\epsilon}{2}[f_\lambda(x_n) + f_\lambda(y_n)], \\ y_{n+1} &= (1-\epsilon)f_\lambda(y_n) + \frac{\epsilon}{2}[f_\lambda(x_n) + f_\lambda(y_n)], \end{aligned} \tag{1}$$

where $f_\lambda(z)=1-\lambda z^2$. In both equations, the second term represents the average coupling term of the two chaotic elements. This model corresponds to a two-dimensional case of globally coupled logistic maps [21]. Equation (1) includes two parameters λ and ϵ corresponding to the nonlinearity of the single logistic map and the coupling strength, respectively. For all parameter values, Eq. (1) has a symmetry with respect to the diagonal that is invariant under the transformation S_d: $(x,y)\mapsto(y,x)$ where $T\circ S_d = S_d \circ T$. Therefore, if there is an attracting region above the diagonal, then its symmetric counterpart necessarily exists below the diagonal, and vice versa.

It is useful for understanding this simple model to consider its geometric properties. Figure 1 schematically illustrates the transformation T for the phase plane in the case of no coupling, i.e., $\epsilon=0$. It should be recalled that the single logistic map consists of a pair of operations, stretch and fold, for an interval. By the two-dimensional transformation T, the phase plane is two-dimensionally stretched, and then folded along the vertical axis and the horizontal axis, respectively, as shown in Fig. 1. Since the transformed phase plane does not cover the whole phase plane, it is divided into two open regions Z_4 (gray) and Z_0 (white). A point X in Z_4 has four preimages X_i^{-1} $(i=1,2,3,4)$, while any point in Z_0 has no preimages. According to the classification based on the number of preimages, the transformation T is a noninvertible map of the (Z_0-Z_4) type [14]. The geometric property of the model with $\epsilon=0$ also gives a hint in understanding the model with $\epsilon\neq 0$. The inverse maps defined for a point $(x,y)\in Z_4$ are given as follows:

$$T_1^{-1}:(x,y)\mapsto(g(x,y),h(x,y)), \tag{2}$$

$$T_2^{-1}:(x,y)\mapsto(g(x,y),-h(x,y)), \tag{3}$$

$$T_3^{-1}:(x,y)\mapsto(-g(x,y),-h(x,y)), \tag{4}$$

$$T_4^{-1}:(x,y)\mapsto(-g(x,y),h(x,y)), \tag{5}$$

where

$$g(x,y)=\sqrt{\frac{1}{2\lambda}\left\{2-\left(1+\frac{1}{1-\epsilon}\right)x-\left(1-\frac{1}{1-\epsilon}\right)y\right\}},$$

$$h(x,y)=\sqrt{\frac{1}{2\lambda}\left\{2-\left(1-\frac{1}{1-\epsilon}\right)x-\left(1+\frac{1}{1-\epsilon}\right)y\right\}}.$$

With these notations, the relation between a point X and its rank-1 preimage X_i^{-1} is described as $X_i^{-1}=T_i^{-1}(X)$ for $i=1,\ldots,4$. In a similar way, a rank-k preimage of a point X is denoted by $X_{i_1 i_2 \cdots i_k}^{-k}=T_{i_1 i_2 \cdots i_k}^{-k}(X)\equiv T_{i_k}^{-1}\circ T_{i_{k-1}}^{-1}\circ\cdots\circ T_{i_1}^{-1}(X)$ where $i_j=1$, 2, 3, or 4 for $j=1,2,\ldots,k$, if it exists. The union of all rank-k preimages of a point X (an area U) is indicated by $T^{-k}(X)$ $[T^{-k}(U)]$.

The curve L (lines in this case) separating the phase plane into the two regions Z_4 and Z_0 is called a *critical curve* of rank 1 [14]. The critical curve is generally an image of L_{-1} given as the locus of points where the Jacobian determinant vanishes. Since L_{-1} is the union of the two axes in Eq. (1), i.e., $L_{-1}=\{(x,y)|x=0 \text{ or } y=0\}$, the critical curve is given as the union of the two half lines as follows:

$$L = \left\{ (x,y) \,\middle|\, y = 1 + \frac{\epsilon}{2-\epsilon}(x-1) \ (x \leqslant 1, y \leqslant 1) \right.$$

$$\left. \text{or } x = 1 + \frac{\epsilon}{2-\epsilon}(y-1) \quad (x \leqslant 1, y \leqslant 1). \right\} \tag{6}$$

It should be noted that the origin O, which is the intersection of the two axes, is mapped into the end point C of the two half lines of L. In Secs. IV and V, the critical curve is used to analyze basin bifurcations [14], i.e., qualitative changes in basin structures.

III. BIFURCATIONS OF THE OFF-DIAGONAL ATTRACTORS

In this section, we investigate a sequence of bifurcations leading to two mutually symmetric off-diagonal chaotic attractors using Kawakami's method [22]. The parameter region where the two off-diagonal attractors coexist is specified. In the following, a local bifurcation of a fixed point or a periodic cycle on the diagonal is called *transverse* if the eigenvalue of the Jacobian matrix with absolute value 1 corresponds to the eigenvector in a direction orthogonal to the diagonal, and *nontransverse* if the direction is parallel to the diagonal. A chaotic attractor consisting of p distant pieces is called a p-periodic chaotic attractor.

We consider bifurcations in the parameter space $\{(\lambda,\epsilon)|0<\lambda<2, 1<\epsilon<2\}$, because a trajectory diverges in the single logistic map if $\lambda>2$ and the transformation T is symmetric with respect to the line $\epsilon=1$ in the parameter plane as follows. Now we write the map T as $T_{\lambda,\epsilon}$ to specify its dependence on the system parameters. Since the relation $T_{\lambda,2-\epsilon}=S_d \circ T_{\lambda,\epsilon}$ holds for all parameter values, it follows that

$$T^2_{\lambda,2-\epsilon} = (S_d \circ T_{\lambda,\epsilon}) \circ (S_d \circ T_{\lambda,\epsilon}) = S_d \circ S_d \circ T_{\lambda,\epsilon} \circ T_{\lambda,\epsilon} = T^2_{\lambda,\epsilon} \tag{7}$$

from the properties of the transformation S_d, i.e., $T \circ S_d = S_d \circ T$ and $S_d \circ S_d = I$ where I is the 2×2 unit matrix. Due to the symmetry in Eq. (7), the bifurcation diagram of T^2 in the (λ,ϵ) plane is symmetric with respect to the line $\epsilon=1$. However, there is a little difference between $T_{\lambda,\epsilon}$ and $T_{\lambda,2-\epsilon}$ regarding the symmetry in the phase plane. For instance, there is a pair of two mutually symmetric chaotic attractors when $(\lambda,\epsilon)=(1.67,1.9)$, while there is a two-piece chaotic attractor when $(\lambda,\epsilon)=(1.67,0.1)$. If the two chaotic attractors in the former case are denoted by A_Q and A_R, then the two pieces in the latter case are given as A_Q and A_R. Nevertheless, bifurcations in both cases are essentially the same due to the symmetry in Eq. (7). Thus, we consider the parameter region with $\epsilon>1$, since coexistence of two attractors is convenient for observation of a basin boundary.

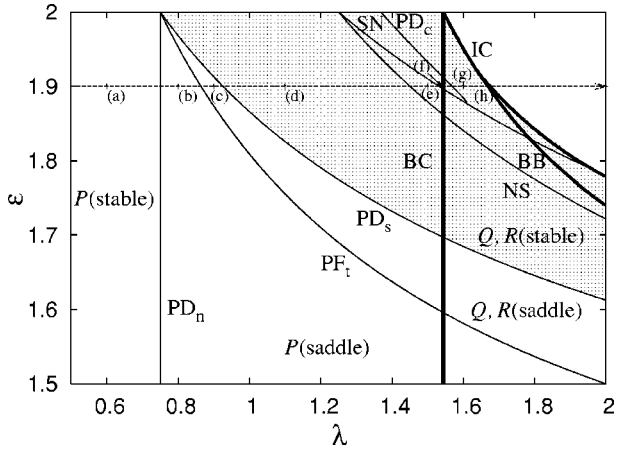

FIG. 2. Bifurcation diagram showing how a pair of two attractors out of the diagonal appears and develops. The gray region indicates the parameter region where the two off-diagonal attractors coexist. The bifurcation sets are denoted as follows: PD_n, nontransverse period-doubling bifurcation of P; PF_t, transverse pitchfork bifurcation of P; PD_s, subcritical period-doubling bifurcations of Q and R; NS, Neimark-Sacker bifurcations of Q and R; SN, saddle-node bifurcations on the invariant circles; PD_c, period-doubling bifurcations of the four-periodic cycles. The phase plots at the parameter values denoted by (a)–(h) are shown in Figs. 3(a)–3(h). The bold curves BC, BB, and IC indicate basin bifurcation sets (see Fig. 7 for details).

Figure 2 shows bifurcation sets related to the two off-diagonal attractors. The gray region indicates the parameter region where the two attractors coexist. For simplicity, we explain the bifurcation scenario leading to the two chaotic attractors along the dashed arrow in Fig. 2, where ϵ is fixed at 1.9. Phase plots at the parameter values denoted by (a)–(h) in Fig. 2 are correspondingly shown in Figs. 3(a)–3(h).

$(a)\rightarrow(b)$. When $\lambda<0.75$, there is a stable fixed point $P=(x_P,y_P)$ on the diagonal, where

$$x_P = y_P = \frac{-1+\sqrt{1+4\lambda}}{2\lambda}. \tag{8}$$

The stable fixed point P changes into a saddle fixed point and a two-periodic cycle P^2 emerges on the diagonal through the nontransverse period-doubling bifurcation (PD_n in Fig. 2).

$(b)\rightarrow(c)$. The saddle fixed point P turns into a repelling fixed point via the transverse pitchfork bifurcation (PF_t in Fig. 2) at $\lambda=(2\epsilon-1)/4(1-\epsilon)^2$. The pitchfork bifurcation generates a pair of mutually symmetric saddle fixed points, $Q=(x_Q,y_Q)$ below the diagonal and $R=S_d(Q)=(y_Q,x_Q)$ above that, where

$$x_Q = \frac{-1+\sqrt{1-2\epsilon+4\lambda(1-\epsilon)^2}}{2\lambda(1-\epsilon)}, \tag{9}$$

$$y_Q = \frac{-1-\sqrt{1-2\epsilon+4\lambda(1-\epsilon)^2}}{2\lambda(1-\epsilon)}. \tag{10}$$

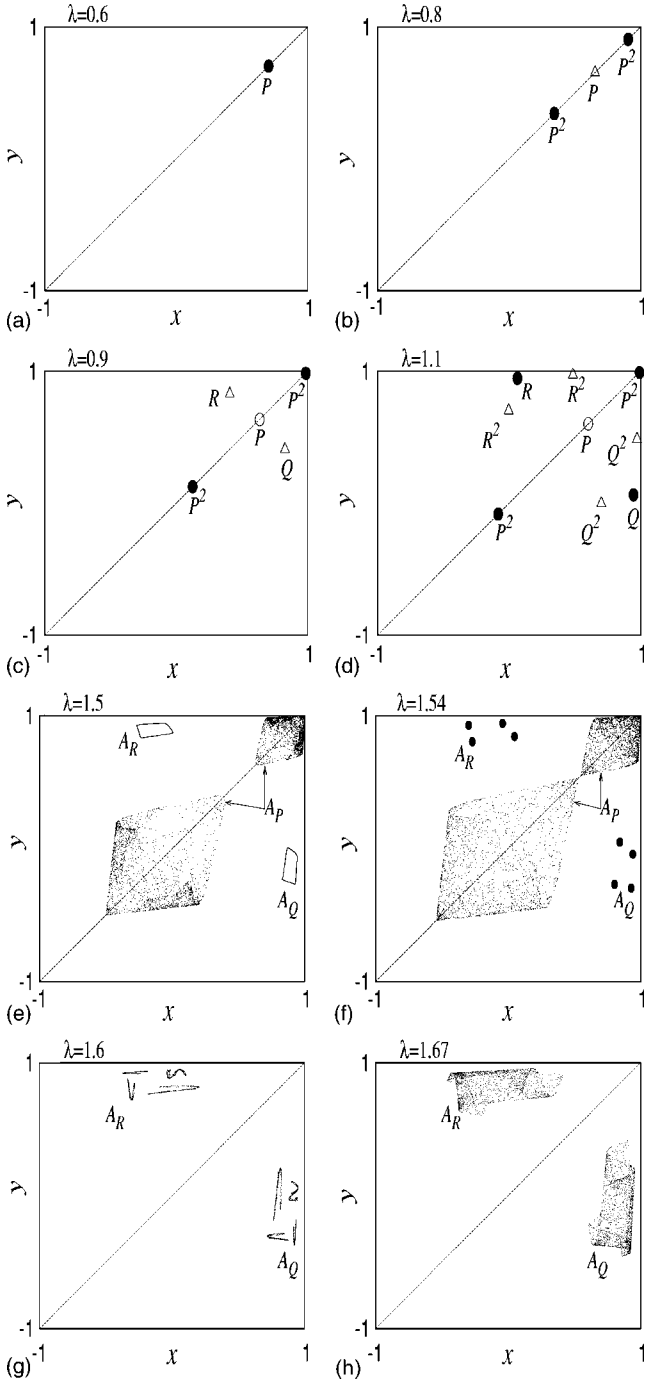

FIG. 3. Phase plots at different values of λ with $\epsilon=1.9$. The filled circles, the triangles, and the open circles indicate stable, saddle, and repelling points, respectively. The off-diagonal attractors are indicated by A_Q and A_R and the other is represented by A_P.

$(c)\rightarrow(d)$. The saddle off-diagonal fixed points recover their stability through the subcritical period-doubling bifurcation (PD_S in Fig. 2). The two-periodic saddle cycles Q^2 and $R^2=S_d(Q^2)$ generated at the bifurcation contribute to the formation of a basin boundary as described in the next section.

$(d)\rightarrow(e)$. The invariant closed curves A_Q and A_R are generated with loss of stability of the stable fixed points Q and R, by the Neimark-Sacker bifurcation (NS in Fig. 2), respectively.

$(e)\rightarrow(f)$. The four-periodic cycles A_Q and A_R emerge through the saddle-node bifurcation (SN in Fig. 2) on the invariant closed curves.

$(f)\rightarrow(g)$. The four-periodic cycles A_Q and A_R develop into four-periodic chaotic attractors through successive period-doubling bifurcations (the first one is denoted by PD_C in Fig. 2). The transition from (e) to (g) is a typical torus-breaking route to chaos [23].

$(g)\rightarrow(h)$. Each four-periodic chaotic attractor merges into a one-piece chaotic attractor through a global bifurcation.

The sequence of bifurcations of attractors described above is similar to that in the system of two logistic maps with linear coupling [23,24]. In our model, the two off-diagonal chaotic attractors suddenly merge into a larger chaotic attractor by simultaneous interior crises (IC in Fig. 2). The attractor-merging crisis gives rise to intermittent transitions between two distant regions that are originally attracting. Since a crisis is generally caused by a contact between an attractor and its basin boundary [20], it is needed for understanding of the attractor-merging crisis to analyze not only bifurcations of the attractors but also changes of their basin boundary. Thus, we focus on the formation of the basin structure and the basin bifurcations in the next two sections.

IV. FORMATION OF BASIN BOUNDARY WITH SADDLE CYCLES

In this section, we consider the basin structure and we focus our attention on the immediate basins of the off-diagonal attractors. The total basin of an attracting set A is defined as the set $D=\cup_{k\geq 0}T^{-k}(U)$ where U is some attracting neighborhood of A, while the immediate basin D_0 of A is defined as the largest connected component of D containing A [14]. The total basin of an attractor A is denoted by $D(A)$ and the immediate one by $D_0(A)$. If a region belongs to $D(A)$, then its preimages also belong to $D(A)$.

Figure 4 shows a basin structure under the coexistence of the three attractors, P^2, Q, and R, at the parameter value denoted by (d) in Fig. 2. The corresponding phase plot is also shown in Fig. 3(d). The total basins of P^2, Q, and R are indicated by silver, light gray, and dark gray, respectively. The white region indicates the set of initial conditions with which a trajectory diverges to infinity. By definition, the immediate basin $D_0(Q)$ $[D_0(R)]$ is the connected region including Q (R), which is bounded by the four solid segments. It can be seen in Fig. 4 that $D_0(Q)$ is divided into two regions $D_0(Q)\cap Z_4$ and $D_0(Q)\cap Z_0$ by the critical curve L. It should be noted that $D_0(Q)\cap Z_4$ has preimages while $D_0(Q)\cap Z_0$ has no preimages. The union of the four rank-1 preimages of $D_0(Q)\cap Z_4$ is equivalent to the union of $D_0(Q)$ and its mirror image $D_0'(Q)$ in the opposite side with respect to the axis $x=0$. In a similar way, $T^{-1}(D_0(R)\cap Z_4)=D_0(R)\cup D_0'(R)$ where $D_0'(R)=S_d(D_0'(Q))$. The regions $D_0'(Q)$ and $D_0'(R)$ are bounded by four segments with four cusp points [14], respectively. A cusp point indicates a preimage of the repelling fixed point P. Hence, an isolated component of $D(Q)$ $[D(R)]$,

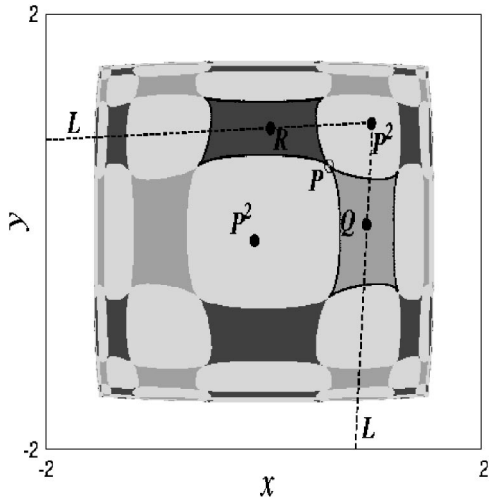

FIG. 4. Basins of attraction of P^2 (silver), Q (light gray), and R (dark gray) where $(\lambda,\epsilon)=(1.1,1.9)$. The white region indicates the set of initial conditions with which a trajectory diverges. The largest connected region including Q (R) represents the immediate basin $D_0(Q)$ [$D_0(R)$].

which is a preimage of $D_0'(Q)$ [$D_0'(R)$], has a boundary consisting of four segments with four cusp points.

Now we explain how the immediate basin $D_0(Q)$ and its basin boundary are formed. As mentioned in Sec. III, the two-periodic saddle cycles Q^2 and R^2 play a significant role in the formation of the basin boundary. Figure 5(a) shows the immediate basin $D_0(Q)$ corresponding to that shown in Fig. 4. The smooth segment PM consisting of the stable invariant sets of Q^2 is the basic element for the immediate basin boundary, where M is the intersection of the invariant set and the critical curve L. It should be noted that Q^2 is very close to M and located on the left-hand side of L. On the other hand, one of the unstable invariant set of Q^2 extends in a direction towards Q in $D_0(Q)$ and the other towards P^2 in the outside of $D_0(Q)$. The unstable invariant set of P below the diagonal also extends in a direction towards Q as shown in Fig. 5. A trajectory starting from an initial condition close to P departs away from it along an integral curve [25]. These integral curves can be locally approximated as the solutions to the linearized map DT in the vicinity of P. This leads to the repelling tongue, which is now cusplike because the local dynamics near P is more expanding in a direction transverse to the diagonal than along the diagonal [25]. The boundary of $D_0(Q)$ is made up of the basic segment PM and its preimages, where the four boundary segments are represented as follows:

$$PP_2^{-1} = T_1^{-1}(PM) \cup T_2^{-1}(PM), \tag{11}$$

$$PP_{21}^{-2} = T_1^{-1}(PP_2^{-1}), \tag{12}$$

$$P_2^{-1}P_{22}^{-2} = T_2^{-1}(PP_2^{-1}), \tag{13}$$

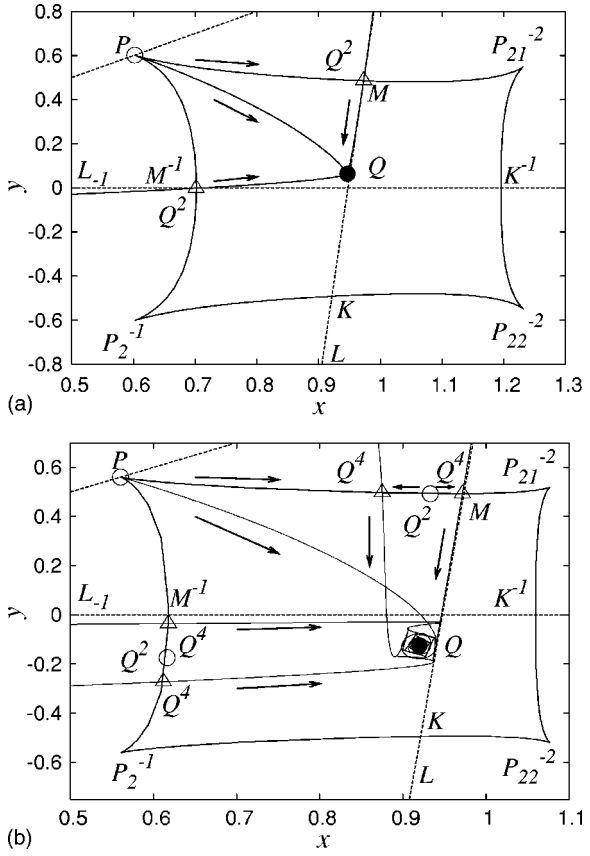

FIG. 5. Boundary of the immediate basin $D_0(Q)$ below the diagonal. It is formed by the segment PM and its preimages. The segment consists of stable invariant sets of a saddle cycle. The saddle cycle is (a) Q^2 where $(\lambda,\epsilon)=(1.1,1.9)$ and (b) Q^4 where $(\lambda,\epsilon)=(1.4,1.9)$. The filled circles, the triangles, and the open circles indicate stable, saddle, and repelling points, respectively. The intersections of L and the immediate basin boundary are denoted by M and K.

$$P_{21}^{-2}P_{22}^{-2} = T_1^{-1}(P_2^{-1}K) \cup T_2^{-1}(P_2^{-1}K), \tag{14}$$

where K is the intersection of the segment $P_2^{-1}P_{22}^{-2}$ and L. Consequently, the boundary of $D_0(Q)$ is formed by the invariant sets of the saddle cycle Q^2 and their preimages.

With variation of the parameter values, the saddle cycle Q^2 undergoes successive period-doubling bifurcations as shown in Fig. 6. Through the period-doubling bifurcation denoted by PD^{2^k}, a 2^k-periodic saddle cycle Q^{2^k} changes into a repelling cycle and a 2^{k+1}-periodic saddle cycle $Q^{2^{k+1}}$ emerges. Figure 5(b) shows the immediate basin boundary at the parameter value denoted by (b) in Fig. 6, where the basic segment PM consists of stable invariant manifolds of Q^4. Accordingly, the smooth boundary of $D_0(Q)$, which is made up of PM and its preimages, still holds. Similarly, the smooth boundary of the immediate basin holds for the period-doubling cascade of the saddle cycles. The cascade leads to a chaotic saddle after its accumulation. Hence, the immediate basin boundary is made up of a chaotic saddle and its preimages after the accumulation of the cascade. However, it is not possible to conclude (at this study level)

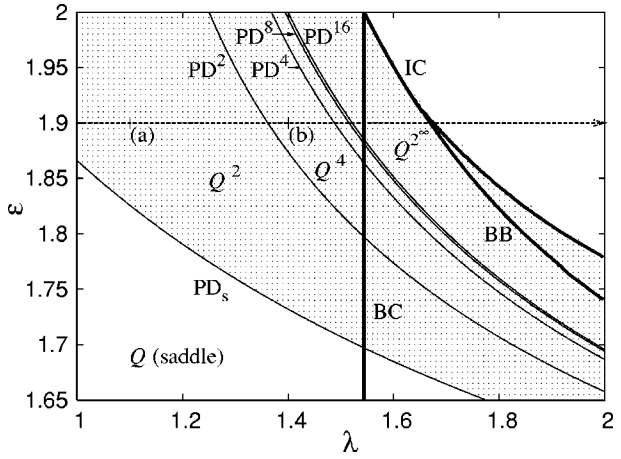

FIG. 6. Successive period-doubling bifurcations of saddle cycles. The period-doubling bifurcation of a saddle cycle Q^{2^k} is denoted by PD^{2^k} ($k=1,2,3,4$). The period-doubling cascade suggests the existence of a chaotic saddle Q^{2^∞}. Immediate basin boundaries at the parameter values denoted by (a) and (b) are shown in Figs. 5(a) and 5(b).

whether the segment PM remains smooth even after the accumulation of the period-doubling cascade (see p. 370 of Ref. [14]).

V. QUALITATIVE AND QUANTITATIVE CHANGES OF FRACTAL BASIN BOUNDARY

In this section, successive changes in basin structures are considered as λ increases along the dashed arrow in Fig. 7. The primary three subsections deal with basin bifurcations including the genesis, changes, and destruction of a fractal basin boundary. These three major changes in basin structures take place at the parameter sets denoted by BC, BB, and IC in Fig. 7, respectively. In the last subsection, the fractal dimension of the basin boundary characterizes these basin bifurcations.

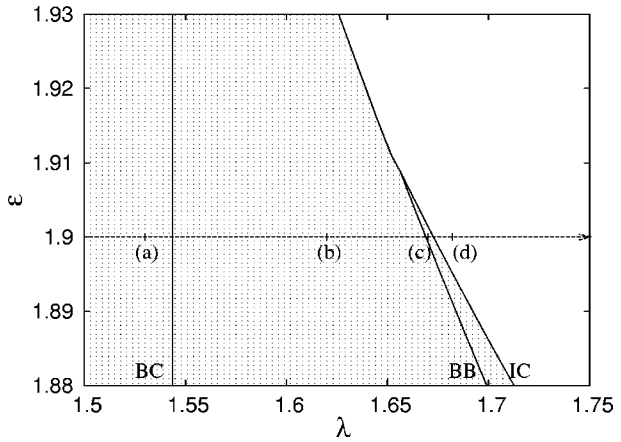

FIG. 7. Phase diagram showing the parameter sets of boundary crisis (BC), basin bifurcation (BB), and interior crisis (IC). Phase plots at the parameter values indicated by (a)–(d) are shown in Figs. 8(a), 8(b), 10(b), and 12, respectively.

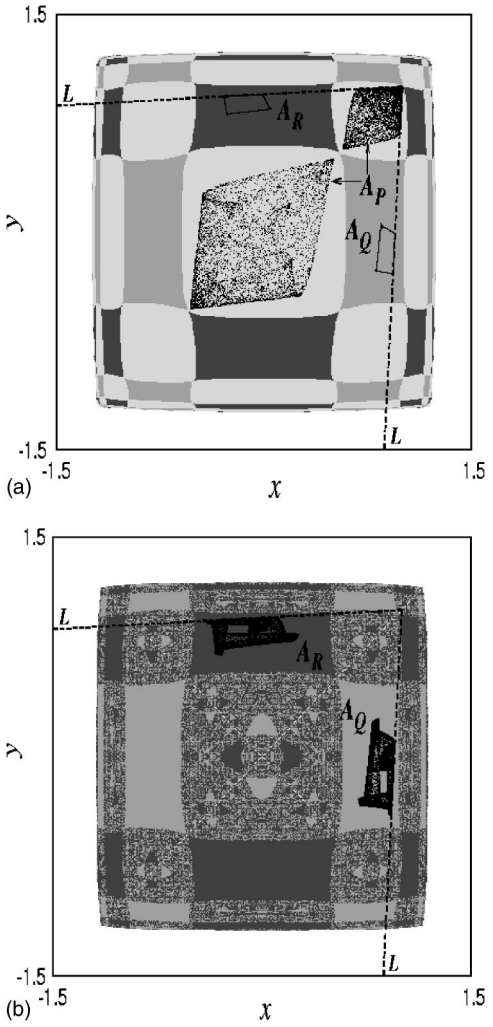

FIG. 8. Basin structures before and after the boundary crisis: (a) total basins of A_P (silver), A_Q (light gray), and A_R (dark gray) where $(\lambda,\epsilon)=(1.53,1.9)$; (b) fractal basin boundary separating the total basins of A_Q (light gray) and A_R (dark gray) where $(\lambda,\epsilon)=(1.62,1.9)$.

A. Genesis

We consider a genesis of a fractal basin boundary at the parameter set of a boundary crisis denoted by BC in Fig. 7. Before the boundary crisis, there are three coexisting attractors A_P, A_Q, and A_R, as shown in Fig. 8(a). The basin structure is qualitatively the same as that in Fig. 4, though the attractors are topologically different. As λ increases, two disjoint sets of the attractor A_P become larger in size and their two end points finally contact at the repelling fixed point P on the basin boundary. The boundary crisis leads to the disappearance of A_P.

The boundary crisis set is specified by considering the dynamics in the diagonal where the model is reduced to the single logistic map. At the boundary crisis, the logistic map exhibits merging of a two-band chaotic attractor into a one-band chaotic attractor. From this fact, the boundary crisis parameter value λ_b satisfies $f^3_{\lambda_b}(0)=x_P$, or

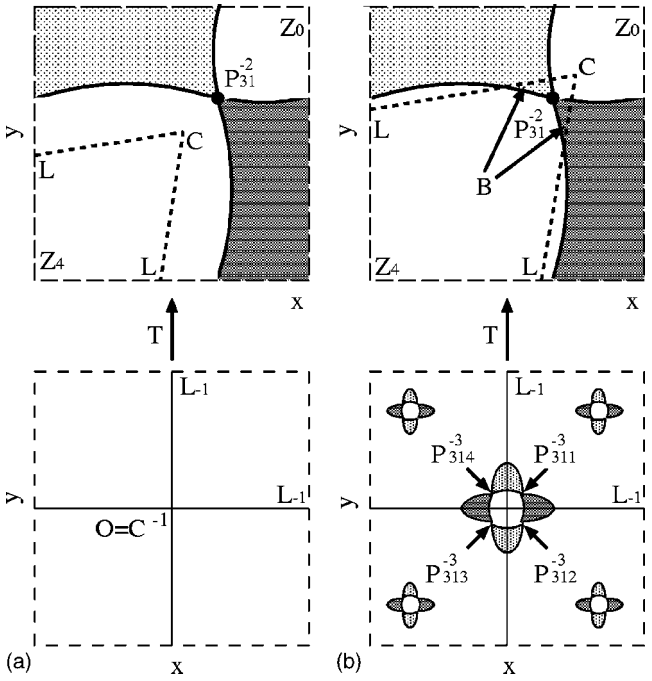

FIG. 9. Schematic illustration of the relations between the basin boundary and the critical curve L, showing a mechanism of the basin fractalization. A point near the origin O (bottom) is mapped into a point near the end point C of the critical curve (upper). (a) The cusp point P_{31}^{-2} belongs to the region Z_0 before the basin fractalization. (b) The four preimages of the region B are present as the four tongues whose closures are connected at the four rank-3 preimages of P after the basin fractalization.

$$\lambda_b^3 - 2\lambda_b^2 + 2\lambda_b - 2 = 0, \tag{15}$$

which gives $\lambda_b \approx 1.543\,68$. Hence, the parameter set of the boundary crisis is independent of the coupling parameter ϵ.

Figure 8(b) shows a basin structure after the boundary crisis of A_P. A fractal basin boundary separating the basins of A_Q and A_R appears in the region that is previously the basin of attraction of A_P. In order to understand the basin fractalization geometrically, we focus on the area near the end point of the two half lines of L. Figure 9 schematically illustrates the relations between the basin boundary and the critical curve L before and after the boundary crisis. The upper figure represents a neighborhood of the end point C, while the bottom one represents a neighborhood of the origin O. It should be recalled that O is the fourfold rank-1 preimage of C. Before the boundary crisis, L is distant from the two segments of the basin boundary connected at P_{31}^{-2} as shown in Fig. 9(a). Since the neighborhood of C belongs to the basin of A_P, the neighborhood of O also belongs to the basin of A_P. At the boundary crisis, C contacts the cusp point P_{31}^{-2} on the basin boundary. A contact between a critical curve and a basin boundary is called a *contact bifurcation* [14], because it brings about a qualitative change in a basin structure. After the contact, L intersects the two segments of the basin boundary, and the rank-1 preimages of the region B appear near the origin as shown in Fig. 9(b). The four tonguelike preimages can be clearly confirmed in Fig. 8(b). The boundaries of the four tongues are connected by the rank-3 preimages of P. The union of the four tongues, $T^{-1}(B)$, has four preimages with a similar shape. If all the preimages of $T^{-1}(B)$ are cut out from the area that is previously the basin of A_P, then only a set of isolated points remains. The fractal set is the basin boundary separating $D(A_Q)$ and $D(A_R)$. Due to the chaotic dynamics in the area, a chaotic repeller is embedded in the fractal basin boundary.

B. Changes

After the genesis of the fractal basin boundary, there are infinitely many preimages of the repelling fixed point P near the end point C of the critical curve. Therefore, as λ increases, the fractal basin boundary successively contacts the critical curve L. This implies that the basin structure successively changes through the contact bifurcations. In fact, the fractal dimension of the basin boundary gradually decreases with increase of λ as shown later. However, the immediate basins $D_0(A_Q)$ and $D_0(A_R)$ remain *simply connected* [14] for the successive minor changes. Further increase of λ gives rise to a qualitative change of the immediate basins.

Figure 10(a) shows a simply connected immediate basin of A_Q. It is bounded by four segments as examined in Sec. IV. The simply connected region changes into a multiply connected one as shown in Fig. 10(b) at the parameter set denoted by BB in Fig. 7. In the multiply connected immediate basin, some points belonging to the basin of A_R (dark gray points) intrude into the previously simply connected region as shown in Fig. 10(c). The immediate basin of A_R also changes into a multiply connected one due to the symmetry. The qualitative change of the immediate basin results from a contact between the boundary of the immediate basin and the critical curve L.

We focus on the upper-right region of $D_0(A_Q)$. The relation between the boundary F and L is illustrated in Fig. 11. Although it is hard to obtain the boundary F precisely, the repelling property of F implies that two neighbor points on different sides of the boundary move away from it in the opposite directions. Using this property, the boundary F is approximately calculated as a boundary separating the two sets of points leaving in opposite directions by iterations of T as shown in Fig. 11. Before the contact, the points on the right-hand side of F have no preimages since L is distant from F as shown in Fig. 11(a). After the contact between L and F, there appears the region H belonging to Z_4 on the left-hand side of L as shown in Fig. 11(b). The region H has preimages in the previously simply connected region. If H had only points belonging to $D(A_R)$, then the preimages of H would look like holes [14,26]. In our case, however, the region H includes points belonging to $D(A_Q)$ as well as those belonging to $D(A_R)$. Consequently, the preimages of H including both the dark and light gray points do not appear to be holes as shown in Fig. 10(c).

Kitajima *et al.* [27] has proposed a method to calculate a parameter set of a basin bifurcation. The algorithm can be used when a basin boundary is made up of stable invariant sets of a saddle cycle. As suggested in Sec. IV, the boundary of $D_0(A_Q)$ consists of a chaotic saddle and its preimages at

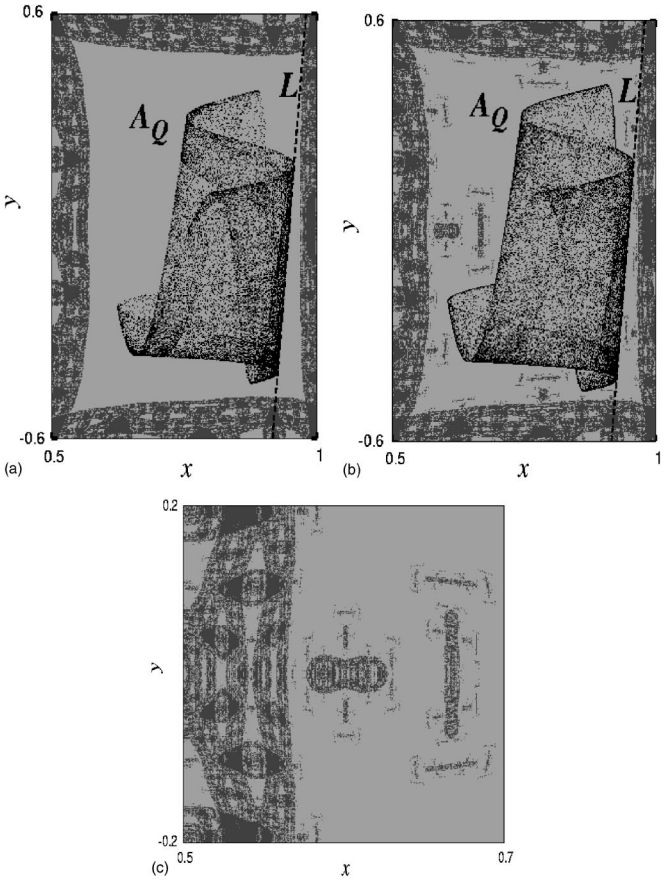

FIG. 10. Immediate basins of A_Q before and after the basin bifurcation: (a) simply connected where $(\lambda, \epsilon) = (1.66, 1.9)$; (b) multiply connected where $(\lambda, \epsilon) = (1.67, 1.9)$; (c) enlargement of the middle part of (b).

the changes of the immediate basins. Hence, the method is not applicable to this case. To roughly estimate the parameter set of the changes of the immediate basins, we prepare a proper region belonging to $D_0(A_Q) \backslash A_Q$, e.g., the right-half region in Fig. 10(c). For a fixed parameter and a number of initial conditions in the proper region, if all trajectories are asymptotic to A_Q, then the parameter value is regarded as that before the basin bifurcation. If at least one of them is asymptotic to A_R, then it is regarded as the parameter value after the basin bifurcation. Using this simple test, we obtain the parameter set denoted by BB in Fig. 7.

C. Destruction

After the change of the simply connected immediate basin into the multiply connected one, the region H in Fig. 11(b) grows in size with further increase of λ. With the growth of H, basin bifurcations successively occur due to successive contacts between the fractal basin boundary and the critical curve L. Accordingly, the preimages of H approach the attractor A_Q, and finally a certain preimage of H contacts it [14]. This is called a contact bifurcation of the first kind [19], which gives rise to a sudden change of multiple distant chaotic attractors into one larger chaotic attractor. The simultaneous contacts between the attractors and the fractal basin

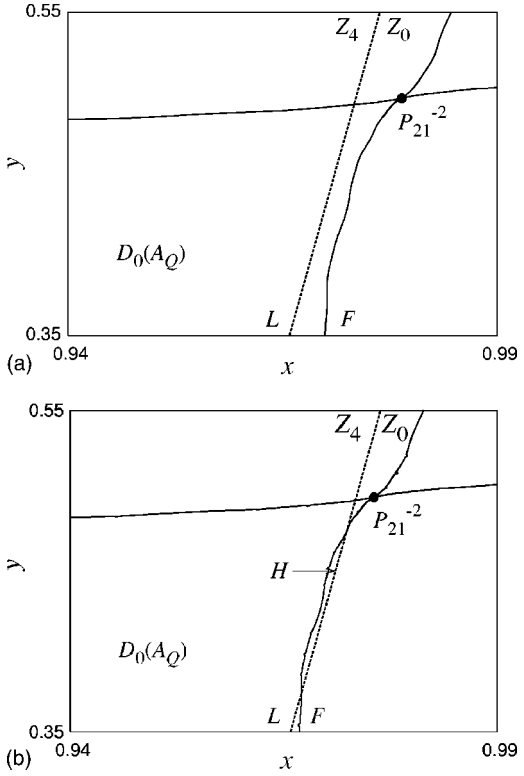

FIG. 11. Relation between the basin boundary F and the critical curve L in the upper-right region of $D_0(A_Q)$.

boundary in both sides of the diagonal result in an abrupt widening of the attractors and a destruction of the basin boundary. The bifurcation can be viewed as an explosion of chaotic sets [28] where the attracting chaotic sets contact a repelling chaotic set embedded in the fractal basin boundary.

To roughly estimate the crisis parameter set, we prepare a proper region belonging to A_Q. For a fixed parameter and a number of initial conditions in the proper region, if all trajectories stay in A_Q for a sufficiently long time then the parameter value is regarded as that before the crisis. Otherwise, it is regarded as the parameter value after the crisis. Using this simple test, we obtain the crisis parameter set denoted by IC in Fig. 7, where it is also observed that the parameter sets denoted by BB and IC merge at $\epsilon \sim 1.91$. This means that the contact occurs between the attractors and the boundary of the immediate basin that is not multiply but simply connected.

Figure 12(a) shows the chaotic attractor, which is generated immediately after the attractor-merging crisis. The crisis can be understood through the unstable invariant manifolds of P. Before the crisis, two unstable manifolds of P extending towards the off-diagonal attractors never intersect. After the crisis, they have infinitely many intersections. Figure 12(b) shows the unstable manifolds of P immediately after the crisis. It can be seen that they return to the neighborhood of P. This implies that the crisis occurs when P first becomes a snap-back repeller [29]. An intersection of the two unstable manifolds means infinitely many intersections of them. Therefore, the intersections enable the everlasting transitions between two distant regions corresponding to the original attractors.

Figure 12(c) shows irregular intermittent behaviors induced by the attractor-merging crisis. A typical trajectory

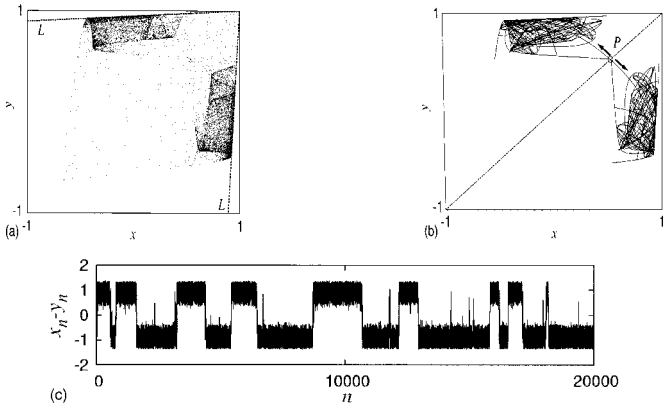

FIG. 12. Crisis-induced intermittency between two distant regions after the attractor-merging where $(\lambda,\epsilon)=(1.682,1.9)$: (a) phase plot; (b) unstable manifolds of P; (c) time series.

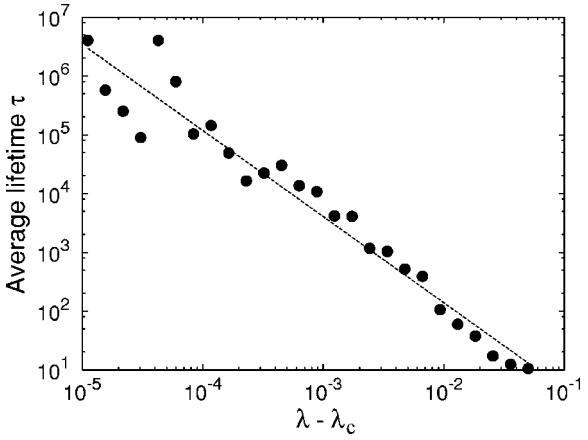

FIG. 13. Dependence of the average lifetime on the parameter λ. The linear fitting indicated by the dashed line yields a critical exponent $\gamma\approx 1.46$ in Eq. (16).

spends a long time in an original attractor region and occasionally moves to the other region. The long lifetime is due to transient chaos [20] related to the chaotic repellers in the originally attracting areas. The frequency of the transitions becomes higher as λ surpasses the crisis parameter value λ_c. In other words, the average lifetime [30] in the transient periods gradually decreases. Figure 13 shows dependence of the average lifetime τ on the parameter λ, which is scaled as follows [12,31]:

$$\tau \sim (\lambda - \lambda_c)^{-\gamma}, \tag{16}$$

for λ close to λ_c. The scaling factor γ is called a *critical exponent* [12]. The scaling properties have been given for two situations of boundary crises including a homoclinic tangency and a heteroclinic tangency [12,31]. In both cases, the scaling properties are characterized by eigenvalues of a Jacobian matrix at a saddle point. In our case, the mechanism of the crisis is different from these two situations. Nevertheless, the average lifetime is scaled with the parameter interval.

D. Fractal dimension

The successive basin bifurcations are characterized by variation of the dimension of the fractal basin boundary. Self-similarity of the fractal basin boundary is clearly observed in Fig. 8(b) where the fractal structure does not disappear no matter how greatly the phase plane is expanded. A fractal basin boundary is a matter of importance since it gives rise to a fundamental difficulty in prediction of the asymptotic behavior of the system due to both the fractal structure with fine-scale complexity and the inevitable small errors in the specification of initial conditions and system parameters [17,32]. An illustrating example of this last idea, showing how the phase space of some prototypical Hamiltonian maps was fractalized, and consequently the predictability of future states was lost, was recently shown in Ref. [33]. Similar ideas applied to Hamiltonians systems are discussed in Ref. [34]. A highly complicated basin structure can be formed due to a fractal basin boundary [26,35] as well as a riddled basin [18,36] and an intermingled basin [25] in noninvertible maps.

A method to characterize a fractal basin boundary is to investigate the uncertainty exponent [17]. For a fractal basin boundary, the probability that several initial conditions with a δ distance apart asymptotically converge to different attractors is scaled with δ as follows:

$$\Pr(\delta) \sim \delta^{\alpha}, \tag{17}$$

where the scaling exponent α with $0<\alpha<1$ is called the uncertainty exponent. The probability $\Pr(\delta)$ represents the fraction that the destination of a trajectory is uncertain for a perturbation ordered by δ. As δ decreases, the uncertainty decreases but a more precise measurement of initial conditions is needed to predict the final state.

To compute the uncertainty exponent of the fractal basin boundary, we choose some values of δ in the range $10^{-11} \leqslant \delta \leqslant 10^{-1}$. For each value of δ, an initial condition (x_0,y_0) is a certainty point if all the final states of the four perturbed initial conditions $(x_0\pm\delta,y_0\pm\delta)$ coincide with that of the nonperturbed initial condition. Otherwise, it is regarded as an uncertainty point. Using 8192 random initial conditions, we obtain the fraction of uncertainty points for δ on a log-log scale as shown in Fig. 14. The uncertainty exponent α is estimated as $\alpha\approx 0.08$ with a linear fitting when $\lambda=1.62$. It has been proved that the fractal basin boundary has a capacity dimension $d=2-\alpha$ for an uncertainty exponent α [17].

Figure 15 shows variation of the fractal dimension of the basin boundary with the change of the parameter λ. As λ increases, the linear fitting of the fraction $\Pr(\delta)$ first succeeds at the genesis of the fractal basin boundary. After that, the dimension roughly decreases through successive contacts between the fractal basin boundary and the critical curve L. The dimension touches the bottom at the major change in the basin structure where simply connected immediate basins turn into multiply connected ones. The dimension increases from the bottom with the development of the points intruding into the previously simply connected regions. Finally, the linear fitting of the fraction $\Pr(\delta)$ fails at the final crisis. Figure 15 illustrates that variation of a dimension of a fractal

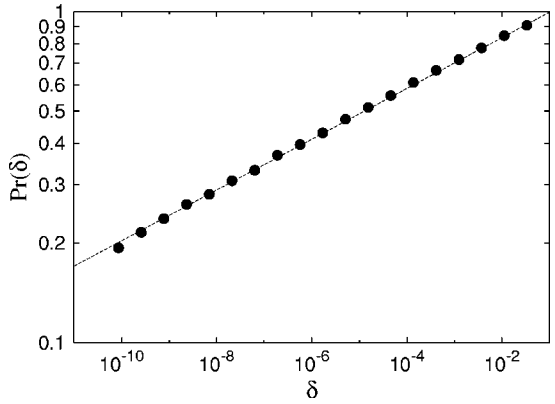

FIG. 14. Scaling property of the fraction of uncertainty initial points for δ in a log-log scale. A linear fitting yields the uncertainty exponent $\alpha \approx 0.08$, where $(\lambda, \epsilon) = (1.62, 1.9)$.

basin boundary can be an informative factor characterizing qualitative changes in the basin structure.

VI. DISCUSSION

We have investigated crisis-induced intermittency in a system of two symmetrically coupled logistic maps. The intermittent behaviors arise through the attractor-merging crisis of two distant attractors that are mutually symmetric. To study the mechanism of the crisis, we have elucidated the topological changes of the attractors and the qualitative changes of their basins with variation of system parameter values. The main three basin bifurcations are the genesis of the fractal basin boundary, the changes of the simply connected immediate basins into the multiply connected ones, and the destruction of the basins with the merging of the attractors. The qualitative changes in the basin structure including these major changes have been quantitatively characterized by the variation of the dimension of the fractal basin boundary.

The model that we have studied is a symmetrically coupled system. However, the exact symmetry between subsystems does not hold owing to inevitable noise for the parameter values in the physical world. Thus, it is important to investigate the robustness of the intermittent behaviors against a slight parameter mismatch violating the symmetry [37,38]. Let us consider a modified scenario of basin bifurcations in the following system with unbalance of the nonlinearity parameters:

$$x_{n+1} = (1-\epsilon) f_{\lambda_1}(x_n) + \frac{\epsilon}{2}[f_{\lambda_1}(x_n) + f_{\lambda_2}(y_n)],$$
$$y_{n+1} = (1-\epsilon) f_{\lambda_2}(y_n) + \frac{\epsilon}{2}[f_{\lambda_1}(x_n) + f_{\lambda_2}(y_n)], \tag{18}$$

where $\lambda_1 = \lambda + \beta$ and $\lambda_2 = \lambda - \beta$. If the mismatch parameter β is sufficiently small, then the symmetry of the original system is slightly violated.

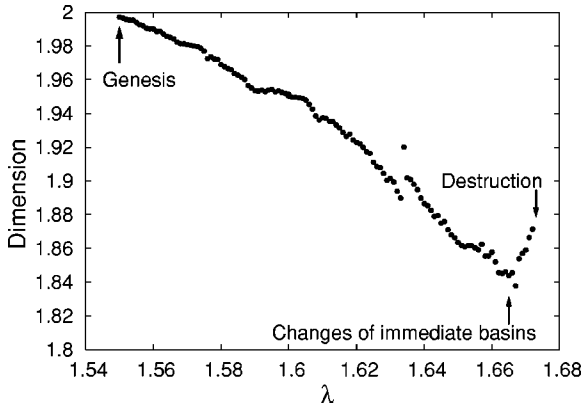

FIG. 15. Fractal dimension with change of λ where $\epsilon = 1.9$. The variation of the dimension characterizes the genesis, the changes, and the destruction of the fractal basin boundary.

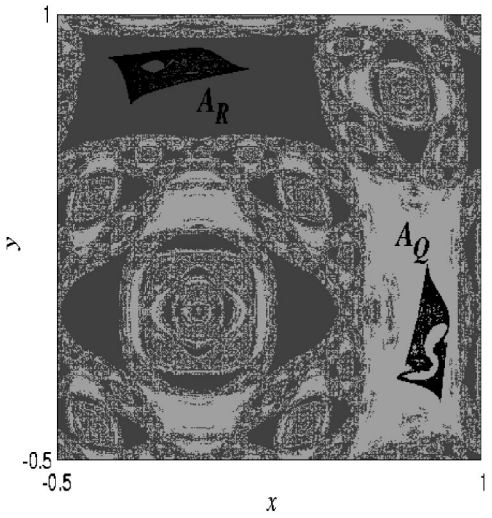

FIG. 16. Basin structure in the asymmetric system (18) where $(\lambda, \epsilon) = (1.8, 1.85)$ and $\beta = 0.01$. The immediate basin of A_R is simply connected whereas that of A_Q is multiply connected.

Due to the asymmetry of the system, the off-diagonal attractors are not mutually symmetric. However, each attractor has a simply connected immediate basin similar to that as shown in Fig. 8(a). When λ increases, the basin fractalization occurs due to the same mechanism as in the symmetric case. There remain only the two attractors A_Q and A_R. The basin structure is similar to Fig. 8(b) after the basin fractalization. With further increase of λ, one of the simply connected immediate basins first changes into a multiply connected one as shown in Fig. 16. The immediate basin of A_Q is already multiply connected, while that of A_R is still simply connected. A similar change of the immediate basin of A_R needs further increase of λ. Therefore, the attractor A_Q first disappears due to an interior crisis caused by a contact between A_Q and the basin boundary. After the crisis, a trajectory with an initial condition near the original attractor A_Q shows transient chaos and finally converges to the only attractor A_R. The last event is the interior crisis of A_R, which brings about a sudden attractor widening [12]. Immediately after the final crisis, intermittent transitions are observed because transient chaos still remains in both originally attracting regions. Con-

sequently, the crisis-induced intermittency is robust against the small parameter mismatch, though the scenario of basin bifurcations is slightly different.

The coupled systems that we have studied can be considered as very simple cases of globally coupled chaotic maps [21,39]. A complicated basin structure with a fractal basin boundary is formed and a contact bifurcation involving the basin boundary brings about a sudden appearance of intermittent transitions even in such simple systems. This may imply that a contact bifurcation involving a basin boundary separating multiple basins of attraction gives rise to intermittent behaviors among multiple distant regions in higher-dimensional coupled maps. Therefore, the results in this paper can be useful for a better understanding of chaotic itinerancy that is typically found in a wide class of such systems [6].

ACKNOWLEDGMENTS

The authors thank H. Kawakami, T. Yoshinaga, and H. Kitajima for their valuable comments and useful discussions. M.A.F.S. acknowledges financial support from the Spanish Ministry of Science and Technology under Projects No. BFM2000-0967 and No. BFM2003-03081, and warm hospitality during his stay in Tokyo. This study is partially supported by the Superrobust Computation Project in the 21st Century COE Program of the Japanese Government.

[1] E. Mosekilde, Y. Maistrenko, and D. Postnov, *Chaotic Synchronization—Applications to Living Systems*, Nonlinear Science Series Vol. A42 (World Scientific, Singapore, 2002).
[2] G.-I. Bischi and L. Gardini, Phys. Rev. E **58**, 5710 (1998).
[3] V. Astakhov, A. Shabunin, T. Kapitaniak, and V. Anishchenko, Phys. Rev. Lett. **79**, 1014 (1997).
[4] Y. L. Maistrenko, V. L. Maistrenko, O. Popovych, and E. Mosekilde, Phys. Rev. E **60**, 2817 (1999).
[5] I. Tsuda, Behav. Brain Sci. **24**, 793 (2001).
[6] K. Kaneko and I. Tsuda, Chaos **13**, 926 (2003).
[7] *Chaotic Itinerancy*, focus issue of Chaos **13**, 926 (2003).
[8] H. Kitajima, T. Yoshinaga, K. Aihara, and H. Kawakami, Chaos **13**, 1122 (2003).
[9] T. Yoshinaga and H. Kawakami, Nonlinear Anal. Theory, Methods Appl. **47**, 5357 (2001).
[10] M. Adachi and K. Aihara, Neural Networks **10**, 83 (1997).
[11] K. Aihara, T. Takabe, and M. Toyoda, Phys. Lett. A **144**, 333 (1990).
[12] C. Grebogi, E. Ott, F. Romeiras, and J. A. Yorke, Phys. Rev. A **36**, 5365 (1987).
[13] E. Ott, *Chaos in Dynamical Systems*, 2nd ed. (Cambridge University Press, Cambridge, U.K., 2002).
[14] C. Mira, L. Gardini, A. Barugola, and J.-C. Cathala, *Chaotic Dynamics in Two-Dimensional Noninvertible Maps*, Nonlinear Science Series Vol. A20 (World Scientific, Singapore, 1996).
[15] C. Grebogi, E. Ott, and J. A. Yorke, Physica D **24**, 243 (1987).
[16] R. Abraham, L. Gardini, and C. Mira, *Chaos in Discrete Dynamical Systems (A Visual Introduction in Two Dimensions)*, (Springer, New York, 1997).
[17] W. McDonald, C. Grebogi, E. Ott, and J. A. Yorke, Physica D **17**, 125 (1985).
[18] Y. Maistrenko, I. Sushko, and L. Gardini, Chaos, Solitons Fractals **9**, 1373 (1998).
[19] C. Mira, C. Rauzy, Y. Maistrenko, and Y. Sushko, Int. J. Bifurcation Chaos Appl. Sci. Eng. **6**, 2299 (1996).
[20] C. Grebogi, E. Ott, and J. A. Yorke, Physica D **7**, 181 (1983).
[21] K. Kaneko, Physica D **41**, 137 (1990).
[22] H. Kawakami, IEEE Trans. Circuits Syst. **CAS-31**, 246 (1984).
[23] K. Kaneko, *Collapse of Tori and Genesis of Chaos in Dissipative Systems* (World Scientific, Singapore, 1986).
[24] L. Gardini, R. Abraham, R. J. Record, and D. F. Prunaret, Int. J. Bifurcation Chaos Appl. Sci. Eng. **4**, 145 (1994).
[25] Y. L. Maistrenko, V. L. Maistrenko, A. Popovich, and E. Mosekilde, Phys. Rev. E **57**, 2713 (1998).
[26] R. L. Ruiz and D. F. Prunaret, Int. J. Bifurcation Chaos Appl. Sci. Eng. **13**, 287 (2003).
[27] H. Kitajima, H. Kawakami, and C. Mira, Int. J. Bifurcation Chaos Appl. Sci. Eng. **10**, 2001 (2000).
[28] C. Robert, K. T. Alligood, E. Ott, and J. A. Yorke, Physica D **144**, 44 (2000).
[29] F. R. Marotto, J. Math. Anal. Appl. **63**, 199 (1978).
[30] B.-L. Hao, *Experimental Study and Characterization of Chaos*, Directions in Chaos Vol. 3 (World Scientific, Singapore, 1990).
[31] C. Grebogi, E. Ott, and J. A. Yorke, Phys. Rev. Lett. **57**, 1284 (1986).
[32] C. Grebogi, S. W. McDonald, E. Ott, and J. A. Yorke, Phys. Lett. **99A**, 415 (1983).
[33] M. A. F. Sanjuan, T. Horita, and K. Aihara, Chaos **144**, 333 (2003).
[34] J. Aguirre and M. A. F. Sanjuan, Phys. Rev. E **67**, 056201 (2003).
[35] M. Inoue and Y. Nishi, Prog. Theor. Phys. **95**, 685 (1996).
[36] O. Popovych, Y. Maistrenko, E. Mosekilde, A. Pikovsky, and J. Kurths, Phys. Rev. E **63**, 036201 (2001).
[37] V. Astakhov, M. Hasler, T. Kapitaniak, A. Shabunin, and V. Anishchenko, Phys. Rev. E **58**, 5620 (1998).
[38] A. Jalnine and S.-Y. Kim, Phys. Rev. E **65**, 026210 (2002).
[39] K. Kaneko, Physica D **54**, 5 (1991).